A Simple Finite Volume Approach to Compute Flows in Variable Cross-Section Ducts

Bruno Audebert, Jean-Marc Hérard, Xavier Martin, Ouardia Touazi

A simple Finite Volume approach to compute flows in variable cross-section ducts

Bruno Audebert and Jean-Marc Hérard and Xavier Martin and Ouardia Touazi

Abstract In order to derive a simple one-dimensional approach that could handle fluid flows in smooth ducts as well as in ducts of discontinuous cross-section, we propose herein a Finite Volume approach that relies on an integral formulation of the multidimensional flow model. While focusing on Euler equations, we compare two-dimensional results with approximations obtained using the present approach, and also with the classical formulation for variable cross-sections using a well-balanced scheme. Numerical simulations confirm the ability of this integral method to provide approximations that compare well with 2D results. This method also enables to deal with all -even including vanishing- cross-section ducts. This approach may also be applied when considering other single-phase or multi-phase fluid flow models.

1 Introduction

Numerical tools devoted to the computation of single-phase or two-phase flows in ducts with variable cross sections are very useful in industry, because they enable to obtain a reasonable approximation of the true flow in unsteady situations, using standard computers. This is of particular interest for hydraulic circuits, as well as in some medecal applications, however it requires the ability to deal with smooth or discontinous cross sections. When neglecting viscous effects and external forces, the classical approach which is overwhelmingly retained consists of constructing numerical approximations of solutions of systems that take the form:

Bruno Audebert, Ouardia Touazi
EDF R&D, Fluid Dynamics, Power Energy and Environment, 6 quai Watier, F78400, Chatou. e-mail: bruno.audebert@edf.fr, ouardia.touazi@edf.fr

Jean-Marc Hérard, Xavier Martin
EDF R&D, Fluid Dynamics, Power Energy and Environment, 6 quai Watier, F78400, Chatou, and: Laboratoire d'Analyse Topologie Probabilités, UMR CNRS 7353, 39 rue Joliot Curie, F13453 Marseille cedex 13. e-mail: jean-marc.herard@edf.fr, xavier-x.martin@edf.fr

$$\begin{array}{l} \dfrac{\partial S}{\partial t} = 0 \\ \dfrac{\partial \rho S}{\partial t} + \dfrac{\partial \rho u S}{\partial x} = 0 \\ \dfrac{\partial \rho u S}{\partial t} + \dfrac{\partial \rho u^2 S}{\partial x} + S\dfrac{\partial P}{\partial x} = 0 \\ \dfrac{\partial E S}{\partial t} + \dfrac{\partial u(E+P)S}{\partial x} = 0 \end{array} \tag{1}$$

where $S(x)$ stands for the area of the cross section, and ρ, u, P, E denote the density, velocity, pressure and total energy of the fluid. Several investigations of the problem that arises with discontinuous cross-sections have been published, among which we may cite [7, 1, 10, 8, 6], wherein authors focus either on the continuous or the discrete framework. Roughly speaking, most of the schemes that have emerged to cope with this problem rely on the well-balanced strategy [5]. The use of this strategy would even seem mandatory; otherwise approximate solutions cansometimes converge towards incorrect solutions (see [8, 3, 6]). Nonetheless, an inconvenience of this strategy is that it assumes that the Riemann invariants of the standing wave associated with $\lambda = 0$ are preserved, which of course makes sense for mass flux and total enthalpy flux, but is questionable in the case of the last Riemann invariant. This has been confirmed by numerical comparisons (see the work reported in [4] for instance), and it is actually quite a well-known problem, the classic treatment for which consists of the introduction of head losses using various empirical closure laws. This problem has motivated the present work, which aims at providing a somewhat different approach in order to eliminate the limitations and drawbacks of the classical approach. Another motivation will be discussed in the conclusion.

The current paper presents the main ideas and results of the work and is organised as follows: firstly, we present the modified one-dimensional approach ; next we present a few numerical results, with a comparison with the two-dimensional approach, the classical approach (1) and the modified one-dimensional formulation, using sufficiently fine enough and reliable meshes.

2 A Finite Volume approach for one-dimensional flows

The one-dimensional formulation is obtained as follows. Starting with the three-dimensional governing equations, restricted here to the Euler framework, thus:

$$(S_2) \left\{ \begin{array}{l} \dfrac{\partial \rho}{\partial t} + \nabla.(\rho \underline{u}) = 0 \\ \dfrac{\partial \rho \underline{u}}{\partial t} + \nabla.(\rho \underline{u} \otimes \underline{u}) + \nabla P = 0 \\ \dfrac{\partial E}{\partial t} + \nabla.(\underline{u}(E+P)) = 0 \end{array} \right.$$

where the total energy E is $E=\rho((\underline{u})^2+\varepsilon(P,\rho))/2$ and $\varepsilon(P,\rho)$ is the internal energy, we integrate over time -from time t^n to t^{n+1}- and space using coarse control volumes as depicted on *Figure 1*. At time $t=t_p$, we denote:

$$\Omega_i^{\varphi}\Phi_i^p=\int_{\Omega_i^{\varphi}}\Phi(\underline{x},t_p)dv$$

for: $\Phi=\rho,\underline{Q},E$ and also $\Omega_i^{\varphi}=S_i\times h_i$ the volume occupied by the fluid within the i-cell. Using previous definitions, and noting Γ_i the boundary of control volume Ω_i, straightforward calculations yield:

$$(S_3)\begin{cases}\Omega_i^{\varphi}\left(\rho_i^{n+1}-\rho_i^n\right)+\int_{[t^n,t^{n+1}]}\int_{\Gamma(i)}(\rho\underline{u}.\underline{n})(\underline{x}_{\Gamma},t)d\Gamma dt=0\\ \Omega_i^{\varphi}\left(\underline{Q}_i^{n+1}-\underline{Q}_i^n\right)+\int_{[t^n,t^{n+1}]}\int_{\Gamma(i)}((\rho\underline{u}.\underline{n})\underline{u}+P\underline{n})(\underline{x}_{\Gamma},t)d\Gamma dt=0\\ \Omega_i^{\varphi}\left(E_i^{n+1}-E_i^n\right)+\int_{[t^n,t^{n+1}]}\int_{\Gamma(i)}((\rho\underline{u}.\underline{n})H)(\underline{x}_{\Gamma},t)d\Gamma dt=0\end{cases}$$

where $\underline{Q}=\rho\underline{U}$ is the momentum and $H=(E+P)/\rho$ is the total enthalpy. Of course, viscous effects and gravity forces could also be included if required.

We may now introduce a simple explicit Finite Volume scheme FVCA (Finite-volumes for Variable Cross-section Applications) as follows:

$$(FVCA)\begin{cases}\Omega_i^{\varphi}\left(\rho_i^{n+1}-\rho_i^n\right)+\Delta t^n\sum_{j\in V(i)}(\rho\underline{u}.\underline{n})_{ij}^h\Gamma_{ij}^{\varphi}=0\\ \Omega_i^{\varphi}\left(\underline{Q}_i^{n+1}-\underline{Q}_i^n\right)+\Delta t^n\sum_{j\in V(i)}((\rho\underline{u}.\underline{n})\underline{u}+P\underline{n})_{ij}^h\Gamma_{ij}^{\varphi}=0\\ \Omega_i^{\varphi}\left(E_i^{n+1}-E_i^n\right)+\Delta t^n\sum_{j\in V(i)}((\rho\underline{u}.\underline{n})H)_{ij}^h\Gamma_{ij}^{\varphi}=0\end{cases}$$

where $(\psi)^h$ stands for some suitable flux scheme (exact or approximate Godunov scheme) associated with the continuous flux ψ, and setting $\Delta t^n=t^{n+1}-t^n$; $V(i)$ refers to the neighbouring cells of cell i and to ghost "mirror" cells associated with the wall boundaries of cell i (see *Figure 1*).

We now assume that the initial condition at time t^n is such that the transverse velocity in the $y-$direction is null everywhere: $U_{y_i}^n=0$. Using the exact Riemann solution for fluxes around all interfaces, and using the mirror technique for all wall boundaries, it may be easily checked that the scalar product of $\underline{e}_y$ with the discrete momentum equation in $(FVCA)$ leads to: $(Q_{y_i}^{n+1}-Q_{y_i}^n)=0$, and thus $Q_{y_i}^{n+1}=0$ or $U_{y_i}^{n+1}=0$. This simply means that the discrete flow remains 1D. We detail now mass and energy balance equations. These read:

$$\Omega_i^{\varphi}\left(\rho_i^{n+1}-\rho_i^n\right)+\Delta t^n\left((\rho u_x)_{i+1/2}^h\Gamma_{i+1/2}^{\varphi}-(\rho u_x)_{i-1/2}^h\Gamma_{i-1/2}^{\varphi}\right)=0 \qquad (2)$$

and :

$$\Omega_i^{\varphi}\left(E_i^{n+1}-E_i^n\right)+\Delta t^n\left((\rho Hu_x)_{i+1/2}^h\Gamma_{i+1/2}^{\varphi}-(\rho Hu_x)_{i-1/2}^h\Gamma_{i-1/2}^{\varphi}\right)=0 \qquad (3)$$

setting $\Gamma^{\varphi}_{i+1/2} = min(S_i, S_{i+1})$. Eventually, the discrete $x-$momentum balance for $Q_x = \rho u_x$ takes the final form:

$$\Omega_i^{\varphi}\left(Q^{n+1}_{x_i} - Q^n_{x_i}\right) + \Delta t^n\Big((\rho u_x^2 + P)^h_{i+1/2}\Gamma^{\varphi}_{i+1/2} - (\rho u_x^2 + P)^h_{i-1/2}\Gamma^{\varphi}_{i-1/2}\Big) + \Delta t^n P^*_{i+\frac{1}{2},i}\left(S_i - \Gamma^{\varphi}_{i+1/2}\right) - \Delta t^n P^*_{i-\frac{1}{2},i}\left(S_i - \Gamma^{\varphi}_{i-1/2}\right)\Big) = 0 \quad (4)$$

where $P^*_{i\pm\frac{1}{2},i}$ is an estimation of the Riemann pressure on the wall boundaries $i \pm 1/2$.

Focusing for instance on perfect gas EOS, hence setting $P = (\gamma - 1)\rho\varepsilon(P,\rho)$, and using classical results (see [2] for example), we obtain when $S_i > S_{i+1}$:

- if $M_i = \frac{u_i^n}{c_i^n} < 0$, then: $P^*_{i+\frac{1}{2},i} = \begin{cases} P_i^n\left(1 + \frac{\gamma-1}{2}M_i\right)^{\frac{2\gamma}{\gamma-1}} & \text{if } 1 + \frac{\gamma-1}{2}M_i \geq 0 \\ 0 & \text{otherwise} \end{cases}$
- if $M_i = \frac{u_i^n}{c_i^n} > 0$, then: $P^*_{i+\frac{1}{2},i} = P_i^n\left(1 + \gamma M_i\left(1 + \frac{(\gamma+1)^2}{16}M_i^2\right)^{1/2} + \frac{\gamma(\gamma+1)}{4}M_i^2\right)$

The same technique is applied when $S_i < S_{i+1}$ in order to estimate $P^*_{i+\frac{1}{2},i+1}$.

On the whole, we can now compute mass, x-momentum and energy balance with the aid of (2),(4),(3), assuming that some standard explicit CFL condition holds for Δt^n. The counterpart of the latter expressions of $P^*_{i\pm\frac{1}{2},i}$ can be found for any EOS, using the mirror state and shock/rarefaction curves in GNL waves. Obviously, there are no intrinsic limits for cross-section values, even if $S_i = 0$. Depending on the choice of numerical fluxes at the fluid interfaces, CFL-like conditions must be introduced in order to guarantee positive discrete values of the density ρ_i^n. Further details can be found in [11].

3 Numerical results

We present in this section a few results arising from a comparison of the three distinct approaches.

- A first approach simply consists of computing the complete set of equations (S2) using the approximate Godunov scheme [2] on a fine enough two-dimensional mesh of about one million cells; the results will be called the reference solution;
- The second series of results were obtained with the classical well-balanced strategy applied to the set of one-dimensional equations (S1), with the focus here on very fine meshes only; the well-balanced Rusanov scheme used in these computations is the one proposed in [8] and also used in [3] where the convergence towards the correct solution has been verified;
- The third series illustrates the numerical approximations obtained by computing the integral system (2),(4),(3) on fine one-dimensional meshes (called $1D+$).

Actually, two slightly different ways of estimating the pressure on the wall boundaries will be applied to the set of formulas above , corresponding respectively to the exact Riemann solution and to the same approximation obtained by setting $M_i = 0$.

The experimental setup is the following: a one dimensional pipe contains a sudden cross-section contraction located at $x = 0.8$ (see Figure 2). At the start of the simulation, a membrane at $x = 0.7$ separates two distinct states $(\rho_L, u_L, P_L) = (1, 0, 10^5)$ and $(\rho_R, u_R, P_R) = (0.125, 0, 10^4)$. Hence, at the beginning, a right-going shock wave followed by a contact discontinuity propagates, then "hits" the cross-section contraction ; this results in a right-going transmitted wave and a left-going reflected wave. We have used a perfect gas EOS setting $\gamma = 7/5$. The fine one-dimensional meshes used for the classical and $1D+$ approaches contain 50000 regular cells, and the CFL number has been set to $1/2$. Two different cross-section ratios are considered, $S_l/S_r = 2$ (figures 3), and $S_l/S_r = 100$ (figures 4 and 5) in test cases 1 and 2 respectively.

Test case 1: $S_l/S_r = 2$: This corresponds to a rather classical situation arising in many practical simulations. We have plotted on Figure 3 the density profiles at time $t = T_0 = 1.5 \times 10^{-3}$; it must be emphasized that the yellow curve refers to some earlier time $t = 0.131 \times 10^{-3}$ when the right-going shock wave had not yet reached $x = 0.8$. As was expected in this particular case, the $1D+$ approximation where M_i is set to 0 -in green- fits experimental "results"- in black- quite well, and performs better than the standard wall-pressure estimation -in red-. The former $1D+$ approach is also much more relevant than the classical approach $(S1)$ using the well-balanced Rusanov scheme ([8])- in blue-.

Test case 2: $S_l/S_r = 100$: Here, the well-balanced Rusanov scheme [8] -in blue- fails to provide approximations on fine meshes, and a similar problem occurs when using the well-balanced approximate Godunov scheme [6]. Thus we were only able to compare results of the multi-dimensional approach to the results provided by the $1D+$ approach (see figures 4 and 5). Both estimations of $P^*_{i\pm\frac{1}{2},i}$ provide similar results, which again was expected, and the comparison with the multi-dimensional approach is even better in this case, which may be explained.

4 Conclusion and further work

The present $1D+$ approach is a very simple one relying on a straightforward integral formulation on particular Finite volumes, combined with an estimation of wall-pressure interactions. We have briefly presented a few of the results from among the sixteen distinct situations that have been investigated up till now, where rarefaction or shock waves interact with eight contractions ($S_l/S_r = 10^{-2}/10^{-1}/0.5/0.9$ and $S_l/S_r = /(0.9)^{-1}/2/10/100$, see [11]). We would like to emphasize that :

- The present approach could be extended in order to take external forces, viscous contributions into account, without any loss of generality;
- The focus here has been on Euler equations but other (single phase or multiphase) fluid flow models could also be considered;
- A key point is that vanishing cross sections may occur in the duct ; furthermore, it must be emphasized that numerical results depend continuously on the cross-section distribution. This can hardly be achieved with the classical approach, at least not when using well-balanced schemes that rely on approximate Godunov schemes. Moreover, even when the classical approach (S1) is feasible, numerical results do not sufficiently match multi-dimensional results.

Another important point is that this method could be extended in order to improve the formulation that is currently applied in a particular three-dimensional porous framework widely used in the nuclear industry (see [9] for instance). We also plan to use the present results in order to improve the basic well-balanced strategy.

Acknowledgements Xavier Martin benefits from financial support through an EDF-CIFRE contract 2012/0838. This work has been achieved within the framework of the TITANS2 project. All computational facilities were provided by EDF. Authors also thank Thomas Pasutto for his help with Code_Saturne.

References

1. Clain, S., Rochette, D.: First and second-order finite volume methods for the one-dimensional non-conservative euler system. Journal of Computational Physics **228**, 8214–8248 (2009)
2. Gallouët, T., Hérard, J.M., Seguin, N.: On the use of symetrizing variables for vacuums. Calcolo **40**(3), 163–194 (2003)
3. Girault, L., Hérard, J.M.: A two-fluid hyperbolic model in a porous medium. ESAIM : Mathematical Modelling and Numerical Analysis **44**(6), 1319–1348 (2010)
4. Girault, L., Hérard, J.M.: Multidimensional computations of a two-fluid hyperbolic model in a porous medium. International Journal on Finite Volumes **7**(1), 1–33 (2010)
5. Greenberg, J.M., Leroux, A.Y.: A well-balanced scheme for the numerical processing of source terms in hyperbolic equations. SIAM Journal on Numerical Analysis **33**(1), 1–16 (1996)
6. Helluy, P., Hérard, J.M., Mathis, H.: A well-balanced approximate riemann solver for compressible flows in variable cross-section ducts. Journal of Computational and Applied Mathematics **236**(7), 1976–1992 (2012)
7. Kröner, D., LeFloch, P., Thanh, M.D.: The minimum entropy principle for compressible fluid flows in a nozzle with discontinuous cross-section. ESAIM : Mathematical Modelling and Numerical Analysis **42**(3), 425–443 (2008)
8. Kröner, D., Thanh, M.D.: Numerical solutions to compressible flows in a nozzle with variable cross-section. SIAM Journal on Numerical Analysis **43**(2), 796–824 (2006)
9. Le Coq, G., Aubry, S., Cahouet, J., Lequesne, P., Nicolas, G., Pastorini, S.: The THYC computer code. A finite volume approach for 3 dimensional two-phase flows in tube bundles. Bulletin de la Direction des études et recherches-Electricité de France. Série A, nucléaire, hydraulique, thermique. In french (1), 61–76 (1989)
10. LeFLoch, P., Thanh, M.D.: The riemann problem for fluid flows in a nozzle with discontinuous cross-section. Communications in Mathematical Sciences **1**, 763–797 (2003)
11. Martin, X.: Numerical modeling of flows in obstructed media. PhD thesis (in preparation)

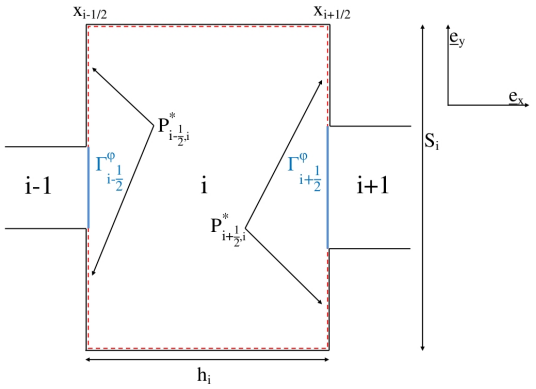

Fig. 1 Finite volume Ω_i with neighbouring cells, fluid interfaces and inner wall-boundaries.

Fig. 2 Experimental setup : 1D pipe with a sudden contraction and position of the initial membrane.

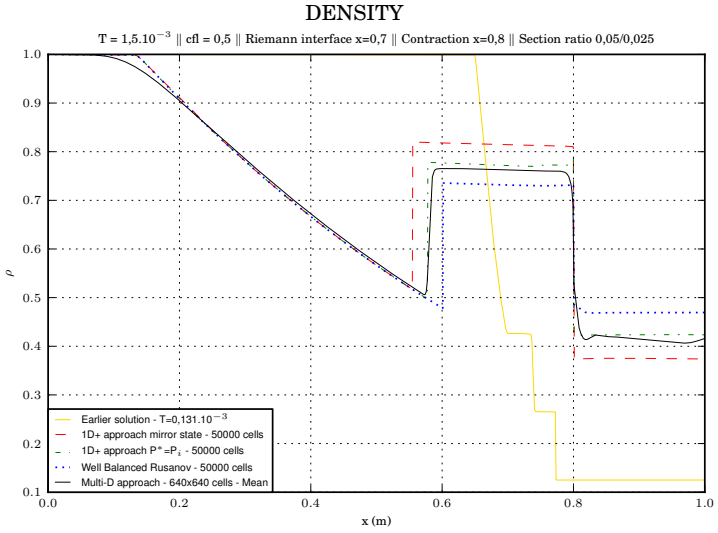

Fig. 3 Density profiles at $t = T_0$ in test case 1. Yellow curve: earlier solution. Dashed red curve: 1D+ approach. Dotted and dashed green curves: 1D+ approach assuming $M_i = 0$ in wall pressures. Dotted blue curve: well-valanced Rusanov scheme. Black curve: $y-$averaging of 2D results.

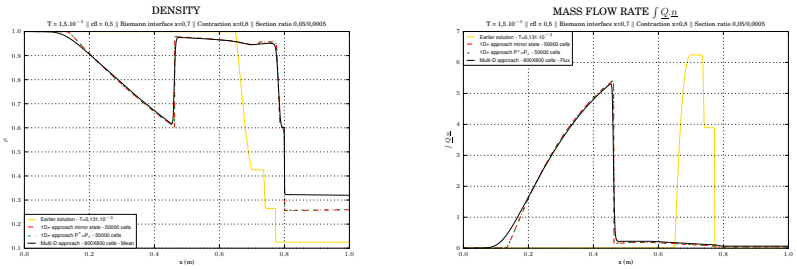

Fig. 4 Density profiles and mass flow rate at $t = T_0$ in test case 2. Yellow curve: earlier solution. Dashed red curve: 1D+ approach. Dotted and dashed green curves: 1D+ approach assuming $M_i = 0$ in wall pressure estimations. Black curve: $y-$averaging of two-dimensional results.

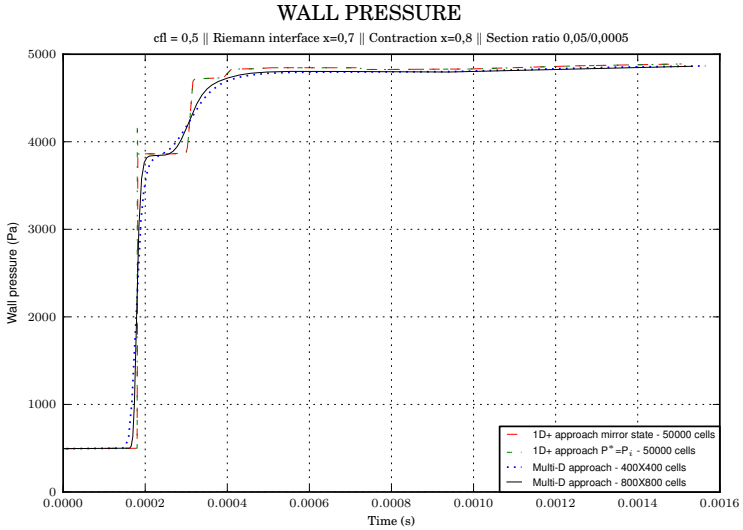

Fig. 5 Comparison of wall pressures. Dashed red curve: 1D+ approach. Dotted and dashed green curves: 1D+ approach setting $M_i = 0$. Dotted blue curve: multidimensional computation using 400^2 cells. Full black curve: multidimensional computation using 800^2 cells.